Compensation of Distorted DWDM Signals by Non-Midway Optical Phase Conjugator in Dispersion-Managed Link Configured with Random-Distributed RDPS

Jae-Pil Chung and Seong-Real Lee *

Posted Date: 27 March 2026

doi: 10.20944/preprints202603.2159.v1

Keywords: dispersion management; dispersion map; non-midway; optical phase conjugator; residual dispersion per span; random distribution; chromatic dispersion; nonlinear Kerr effect; wavelength division multiplexed; Pearson correlation coefficient

 doi:10.20944/preprints202603.2159.v1

Article

Compensation of Distorted DWDM Signals by Non-Midway Optical Phase Conjugator in Dispersion-Managed Link Configured with Random-Distributed RDPS

Jae-Pil Chung [1] and Seong-Real Lee [2,*]

[1] Department of Electronic Engineering, Gachon University, Seongnam 13120, Korea
[2] Division of Navigational Information System, Mokpo National Maritime University, Mokpo 58628, Korea
* Correspondence: reallee@mmu.ac.kr

Abstract

This paper presents a numerical investigation of dispersion-managed dense wavelength division multiplexing (DWDM) transmission systems incorporating a non-midway optical phase conjugator (OPC) under randomly distributed residual dispersion per span (RDPS). Unlike conventional studies assuming ideal symmetric configurations, this work considers more realistic scenarios with asymmetric OPC placement and random dispersion distribution. To ensure the reliability of the analysis, simulations were performed for 100 different random RDPS patterns. A 960 Gb/s DWDM system consisting of 24 channels operating at 40 Gb/s was modeled using the nonlinear Schrödinger equation solved by the split-step Fourier method. To analyze the impact of OPC location, two asymmetric configurations, 23–27 and 27–23, were compared. System performance was evaluated using eye-opening penalty (EOP) and timing jitter (TJ). The results show that OPC location has a significant impact on compensation efficiency, with the 27–23 configuration providing overall better performance than the 23–27 configuration. Although randomly distributed RDPS does not always outperform uniform or deterministic dispersion maps, certain random patterns achieve comparable or even superior compensation performance. Further analysis reveals that high-performing random dispersion maps tend to resemble a half-cycle sinusoidal profile, characterized by positive accumulated dispersion before the OPC and negative accumulated dispersion after the OPC. These findings indicate that partial structural regularity within random dispersion plays a key role in enhancing OPC-based compensation. This study provides practical design guidelines for dispersion-managed optical transmission systems under realistic constraints and suggests that guiding random dispersion distributions toward favorable structures can improve system robustness and flexibility.

Keywords: dispersion management; dispersion map; non-midway; optical phase conjugator; residual dispersion per span; random distribution; chromatic dispersion; nonlinear Kerr effect; wavelength division multiplexed; Pearson correlation coefficient

1. Introduction

The performance of long-haul optical fiber transmission systems is fundamentally constrained by the accumulated interaction between chromatic dispersion and fiber nonlinearities [1]. In dense wavelength-division multiplexing (DWDM) systems employing single-mode fiber (SMF) and erbium-doped fiber amplifiers (EDFAs), these impairments become increasingly severe as transmission distance and launch power increase [2,3]. As a result, quantitative performance

 doi:10.20944/preprints202603.2159.v1

evaluation and optimization of impairment mitigation techniques require systematic and reproducible analysis methods.

Dispersion management (DM) has been widely investigated as an effective means of controlling chromatic dispersion accumulation by properly allocating dispersion-compensating fibers (DCFs) along the transmission link [4–6]. In addition to linear dispersion mitigation, numerical studies have shown that dispersion map configuration strongly influences nonlinear signal distortion in multi-span EDFA-based systems. Accordingly, numerical simulation has become an essential approach for analyzing dispersion-managed links, as it enables controlled evaluation of dispersion distribution effects that are difficult to isolate experimentally.

Optical phase conjugation has also been extensively studied as a technique capable of compensating both chromatic dispersion and nonlinear phase distortion [7–9]. Most previous investigations assume that the optical phase conjugator (OPC) is placed at the exact midpoint of the transmission link, under which symmetric accumulation of impairments before and after the conjugation point can be exploited. Under this midway-OPC assumption, numerical simulations have demonstrated that symmetric dispersion maps significantly enhance compensation efficiency and WDM signal performance.

In dispersion-managed optical transmission links, the configuration of the dispersion map plays a critical role in determining the effectiveness of WDM signal distortion compensation [10,11]. Previous studies have demonstrated that, beyond simple chromatic dispersion cancellation, the longitudinal distribution of dispersion strongly influences the accumulation and compensation of fiber nonlinear impairments in multi-span EDFA-based systems. In particular, numerical investigations have shown that appropriately designed dispersion maps can significantly enhance the symmetry of dispersion and nonlinear phase evolution along the transmission link, thereby improving compensation efficiency when optical phase conjugation (OPC) is employed.

In our previous works, systematic numerical simulations were employed to analyze dispersion-managed links incorporating a midway OPC [12–15]. By intentionally designing dispersion maps with antipodal symmetry, we quantitatively demonstrated improvements in power margin, tolerance to residual dispersion, and nonlinear distortion suppression [12,15]. These results established numerical guidelines for dispersion map optimization under ideal symmetric OPC conditions.

However, in practical optical networks, the placement of an OPC at the exact midpoint of a transmission link is often infeasible due to constraints imposed by network topology, span length variation, and amplifier deployment. From an analytical standpoint, displacement of the OPC from the link center introduces inherent asymmetry in dispersion and nonlinear phase accumulation, rendering conventional midway-optimized dispersion maps suboptimal [16,17].

In dispersion-managed optical transmission links, the configuration of the dispersion map is commonly realized by prescribing the residual dispersion per span (RDPS) in a deterministic or intentionally designed manner. While such artificial RDPS arrangements are useful for elucidating fundamental compensation mechanisms, they often require meticulous span-by-span dispersion control and precise fiber deployment, which is cumbersome and difficult to implement in practical optical networks. Moreover, the assumption of perfectly engineered RDPS distributions deviates from realistic field conditions, where span lengths, fiber parameters, and amplifier locations are inherently nonuniform.

In real transmission systems, residual dispersion is inevitably subject to random fluctuations inherent in manufacturing tolerances, installation constraints, and network reconfiguration. As a result, dispersion maps encountered in practice are more accurately described as randomly distributed rather than ideally structured. Conventional dispersion-map optimization strategies based on intentionally arranged RDPS may therefore overestimate compensation performance and fail to capture the robustness of WDM signal distortion mitigation under realistic operating conditions.

 doi:10.20944/preprints202603.2159.v1

For these reasons, systematic analysis of dispersion-managed links employing randomly distributed RDPS is required. Numerical simulation provides an effective framework for evaluating such random dispersion maps, as it enables statistical characterization of WDM signal distortion and compensation performance without relying on impractical span-by-span dispersion engineering. By investigating dispersion maps with randomized RDPS distributions, more realistic design guidelines can be established for dispersion-managed optical links, particularly in systems incorporating optical phase conjugation under both symmetric and asymmetric link configurations.

In this paper, therefore, we present a comprehensive numerical analysis of dispersion-managed WDM transmission links incorporating a non-midway optical phase conjugator. Time-domain simulations are performed to evaluate the compensation characteristics of various dispersion map configurations under asymmetric OPC placement. System performance is quantitatively assessed in terms of WDM signal distortion and power margin as functions of dispersion parameters and launch power. By directly comparing random-based and fixed RDPS distributions consisting of dispersion maps under identical simulation conditions, this study provides numerically validated insights into dispersion map design strategies suitable for practical, asymmetric OPC-assisted optical transmission systems in dispersion-managed links configured with randomly distributed RDPSs.

2. Modeling Framework for Numerical Simulation

To investigate the transmission characteristics of dispersion-managed optical links incorporating a non-midway OPC, a numerical simulation framework is established for a multi-span DWDM system. The baseline transmission model adopts standard SMF–EDFA configurations widely used in long-haul system analysis, which also allows direct comparison with our previous studies. The modeling objective in this study focuses on asymmetric OPC placement and its resulting dispersion and nonlinear compensation characteristics.

2.1. Transmission Link Configuration

The optical transmission link consists of multiple fiber spans, each composed of SMF, DCF, and EDFA, shown in Figure 1. An OPC is inserted at a predefined location along the link, dividing the transmission path into two unequal sections. Unlike our previous works, where the OPC was constrained to the midpoint of the link to enforce symmetry, the OPC in the present model is intentionally displaced from the midway to create asymmetric transmission conditions. For a total of 50 spans (i.e., $n = 50$), the OPC was asymmetrically positioned either between the 23rd and 24th spans, which is referred to as the 23–27 configuration, or between the 27th and 28th spans, referred to as the 27–23 configuration.

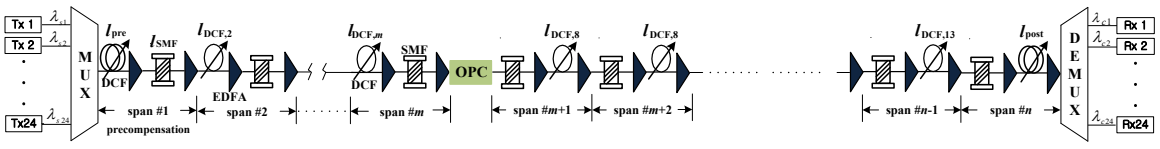

Figure 1. The 960 Gb/s DWDM transmission system through the dispersion-managed link and the non-midway OPC.

We assume SMF parameters as follows: dispersion coefficient is 17 ps/nm/km, attenuation coefficient is 0.2 dB/km, and nonlinear coefficient is 1.41 $W^{-1}km^{-1}$. And DCF is characterized as follows: dispersion coefficient is -100 ps/nm/km, attenuation coefficient is 0.6 dB/km, and nonlinear coefficient is 5.06 $W^{-1}km^{-1}$. These parameter values are assumed for wavelength of 1,550 nm. Although the constituent components of each span are similar to those used in earlier studies, the role of the link configuration in this work is to enable systematic investigation of dispersion imbalance and nonlinear distortion under non-midway OPC placement. This distinction leads to a different

 doi:10.20944/preprints202603.2159.v1

interpretation of dispersion distribution and compensation behavior, even under comparable physical parameters.

2.2. Residual Dispersion Allocation and Definitions

In this study, the RDPS is treated as a flexible design variable rather than a fixed optimization target. This modeling choice differs from our previous work, where the RDPS distribution was constrained to strict antipodal symmetry around the midway OPC. Here, RDPS values are independently and randomly allocated before and after the OPC to analyze their respective compensation characteristics.

In the 27-span optical fiber link, the RDPS of each span was randomly chosen from 27 discrete values between −1300 ps/nm and 1300 ps/nm at 100 ps/nm intervals, determined exclusively by the DCF length in each span. By contrast, in a transmission link consisting of 23 optical fiber spans, the RDPS is randomly selected from one of 23 discrete values ranging from −1320 ps/nm to 1320 ps/nm, separated by 120 ps/nm intervals.

2.3. Dispersion Calibration Strategy

The net residual dispersion (NRD) of each transmission section is defined as the sum of RDPS values assigned to that section. By independently controlling the NRDs of the former transmission sections, the proposed model enables quantitative evaluation of how dispersion asymmetry degrades or modifies OPC-based compensation.

To ensure fair performance comparison across different dispersion configurations, the total residual dispersion of the entire link is maintained near zero. This condition is achieved by introducing a dispersion calibration element at one end of the link. Importantly, this calibration mechanism does not alter the internal RDPS distribution of the transmission spans, thereby preserving the intended asymmetry introduced by non-midway OPC placement.

The purpose of the dispersion calibration technique is consistent with that of the authors' previous studies; however, its objective is not to enforce optimal symmetry, but to regulate the total accumulated residual dispersion of the transmission link to a value close to zero. In this study, as in the previous work, the DCF in the first optical fiber section adjusts the magnitude of the NRD, as indicated by "pre-DC" in Figure 1. Here, "DC" denotes the dispersion calibrator.

2.4. DWDM Transmitters, Receivers, and HNL-DCF–Based OPC Modeling

The DWDM transmission system analyzed in this study is composed of 24 optical channels, each operating at a symbol rate of 40 Gb/s. At the transmitter side, each channel is independently generated using a pseudorandom bit sequence (PRBS) to represent statistically uncorrelated data streams. The electrical data sequence modulates a continuous-wave optical carrier emitted from a distributed feedback laser diode (DFB-LD) via an external intensity modulator, as shown in Figure 2(a).

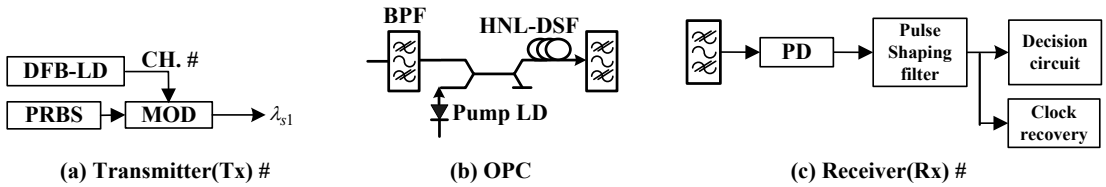

Figure 2. (a) transmitter, (b) OPC, and (c) receiver for 960 Gb/s DWDM transmission.

The optical carrier wavelengths are assigned in accordance with the ITU-T G.694.1 recommendation, covering the range from 1550 nm to 1568.4 nm with a uniform channel spacing of 100 GHz. The modulated optical signals are assumed to be formatted as return-to-zero (RZ) pulses. The pulse shape is modeled as a second-order super-Gaussian waveform with a duty cycle of 0.5 and

 doi:10.20944/preprints202603.2159.v1

a finite extinction ratio, while chirp is neglected for simplicity. The optical signals from the 24 channels are combined using an ideal wavelength multiplexer and subsequently launched into the dispersion-managed transmission link.

The OPC is modeled based on a highly nonlinear dispersion-compensating fiber (HNL-DCF), in which phase conjugation is achieved through a four-wave mixing (FWM) process. The basic configuration of the HNL-DCF OPC is illustrated in Figure 2(b). The incoming DWDM signals interact with a continuous-wave pump wave inside the nonlinear medium, generating phase-conjugated idlers whose spectra are inverted with respect to the pump wavelength. Consequently, the wavelength order of the conjugated channels is reversed relative to that of the transmitted channels.

The HNL-DCF is selected as the nonlinear medium in order to support broadband phase conjugation across the entire DWDM signal bandwidth while allowing control of dispersion within the OPC module. The pump wavelength and power are assumed to be fixed values chosen to ensure stable generation of phase-conjugated waves for all channels. The HNL-DSF parameters are assumed as follows: attenuation coefficient of 0.61 dB/km, nonlinear coefficient of 20.4 $W^{-1}km^{-1}$, a zero-dispersion wavelength of 1,550.0 nm, dispersion slope of 0.032 $ps/nm^2/km$, and length of 0.75 km. After phase conjugation, the WDM signals propagate through the latter half of the transmission link, where the propagation impairments accumulated in the former half are partially compensated under appropriate dispersion and power profile conditions.

At the receiver side, the optical signals are separated by an ideal wavelength demultiplexer and detected using an intensity-modulation/direct-detection (IM/DD) scheme, and the detailed configuration of each receiver is shown in Figure 2(c). Each receiver consists of an optical pre-amplifier, an optical bandpass filter for channel selection, and a PIN photodiode. The detected electrical signal is processed by a low-pass pulse-shaping filter and a decision circuit to recover the transmitted data. The receiver bandwidth is assumed to be a fixed fraction of the symbol rate in order to reflect practical receiver design constraints. The assumptions for simulation are as follows: receiver bandwidth of 0.65 times 40 Gb/s, EDFA with 5 dB noise figure, PIN diode as photodetector, and Butterworth filter as pulse shaping filter.

3. Numerical Analysis and Performance Assessment

3.1. Numerical Modeling

The propagation of optical signals along the transmission link is numerically modeled using the nonlinear Schrödinger equation (NLSE) of Eq. (1), which describes the combined effects of fiber loss, chromatic dispersion, and Kerr nonlinearity in single-mode optical fibers. The NLSE is applied independently to each WDM channel, assuming scalar propagation and neglecting polarization effects. This approach is considered adequate for intensity-modulated DWDM systems operating under relatively large chromatic dispersion, where polarization-dependent interactions play a secondary role.

$$\frac{\partial A_j}{\partial z} = -\frac{\alpha}{2}A_j - \frac{i}{2}\beta_{2j}\frac{\partial^2 A_j}{\partial T^2} + \frac{1}{6}\beta_{3j}\frac{\partial^3 A_j}{\partial T^3} + i\gamma_j\left|A_j\right|^2 A_j + 2i\gamma_j|A_k|^2 A_j, \qquad (1)$$

In the NLSE formulation, linear impairments such as attenuation and group-velocity dispersion are treated together with nonlinear effects arising from the intensity-dependent refractive index of the fiber. Self-phase modulation (SPM) is included as the dominant nonlinear mechanism affecting each channel. Although cross-phase modulation (XPM) may arise in multi-channel WDM transmission, its contribution is assumed to be limited due to significant walk-off between channels induced by chromatic dispersion. Therefore, XPM is not explicitly taken into account in the numerical model in order to reduce computational complexity.

To solve the NLSE, the split-step Fourier (SSF) method is employed. In this method, the transmission fiber is divided into sufficiently small segments, within which linear and nonlinear effects are assumed to act independently. Linear propagation is computed in the frequency domain,

 doi:10.20944/preprints202603.2159.v1

while nonlinear phase accumulation is calculated in the time domain. These two steps are alternately applied along the transmission distance. The step size is selected to ensure numerical stability and convergence of the simulation results. Both SMF and DCF segments are modeled using their respective physical parameters within the same SSF framework.

The OPC is incorporated into the numerical model as an ideal spectral inversion process, consistent with the phase conjugation achieved through four-wave mixing in a highly nonlinear fiber. After the conjugation process, the optical field is spectrally inverted and propagated through the second half of the transmission link using the same NLSE-based approach.

3.2. Performance Metrics

The performance of the received DWDM signals is evaluated using the eye-opening penalty (EOP) and timing jitter (TJ), which are commonly adopted metrics for intensity-modulated optical systems. The EOP is defined as the logarithmic ratio between the eye opening of the received signal and that of a corresponding back-to-back reference signal. The eye opening is obtained from the statistical distribution of the sampled optical power levels, taking into account the minimum level of logical “1” symbols and the maximum level of logical “0” symbols. The EOP provides a quantitative measure of signal degradation caused by dispersion and nonlinear distortions accumulated during transmission.

TJ is used as a complementary performance metric to characterize temporal fluctuations of the received signal. It is evaluated as the deviation of the zero-crossing or decision instant of the received pulses from their ideal timing positions. Excessive TJ indicates pulse distortion and broadening, which may lead to increased inter-symbol interference (ISI) and degraded detection performance. In this study, the TJ is normalized to the symbol duration in order to facilitate comparisons across different transmission conditions.

By jointly analyzing the EOP and TJ, the numerical assessment captures both amplitude-related and timing-related impairments of the DWDM signals, providing a comprehensive evaluation of transmission performance in the dispersion-managed link combined with non-midway OPC.

The authors confirmed their previous findings and applied them in the present study. A common conclusion drawn from earlier investigations is that, when the NRD of dispersion-managed link is adjusted in steps of ±10 ps/nm, a link with NRD set to +10 ps/nm exhibits improved EOP performance compared to other NRD values, whereas a link with NRD set to 0 ps/nm shows superior TJ characteristics. These tendencies were found to be independent of the various dispersion maps considered. Accordingly, in this study, dispersion-managed links with NRD = 10 ps/nm and NRD = 0 ps/nm are employed for EOP analysis and TJ analysis, respectively.

4. Simulation Results and Discussion

Figure 3(a,b) illustrate the difference in power margin based on the EOP evaluation at NRD = 10 ps/nm and the TJ assessment at NRD = 0 ps/nm in the 23-27 configuration and 27-23 configuration, respectively. In this study, the power margin in the EOP evaluation is defined as the range between the maximum and minimum launch powers that result in a 1-dB EOP. Conversely, the power margin in the TJ assessment is defined as the power range where the TJ remains at 25 ps.

 doi:10.20944/preprints202603.2159.v1

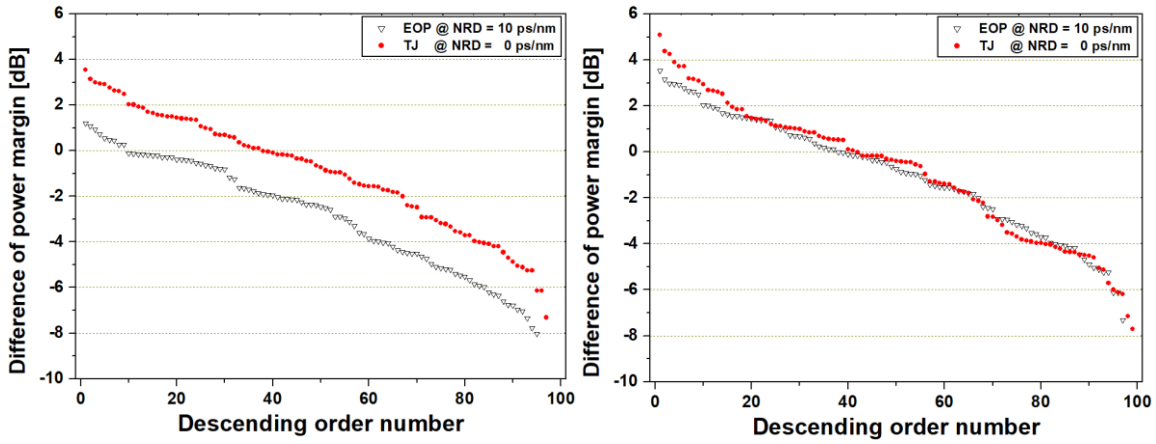

Figure 3. The difference in power margin based on EOP and TJ. (a) 23-27 configuration, and (b) 27-23 configuration.

The "difference of power margin" on the y-axis represents the numerical difference between the power margin obtained from each random pattern and that of a uniform distribution transmission link, in which the RDPS of all fiber spans is fixed at 0 ps/nm. The x-axis in Figure 2, labeled 'descending order number,' indicates that the 100 resulting values are arranged in order of their compensation performance. Specifically, the data points are sorted from the largest to the smallest difference in power margin.

Comparing Figures 3(a) and 3(b), it is evident that the compensation performance is more effectively enhanced when the OPC is positioned closer to the receiver (i.e., the 27-23 configuration) than when it is positioned near the transmitter (i.e., the 23-27 configuration). Furthermore, in the 27-23 configuration, a simultaneous reduction is observed in the deviations of both amplitude compensation (via EOP assessment) and phase compensation (via TJ assessment) for signals distorted by the random distribution of RDPS.

Figure 4 presents the difference in the "product" of launch power and effective NRD. This product is defined as the area of the closed curve formed by the range of effective NRD values that satisfy either an EOP of 1-dB or a TJ of 25-ps across the entire range of applicable launch powers. In this study, this measured area is referred to simply as the "product" and is employed as a quantitative measure to evaluate the design flexibility of dispersion-managed links. A larger product indicates a broader operational window, thereby providing greater tolerance in system configuration.

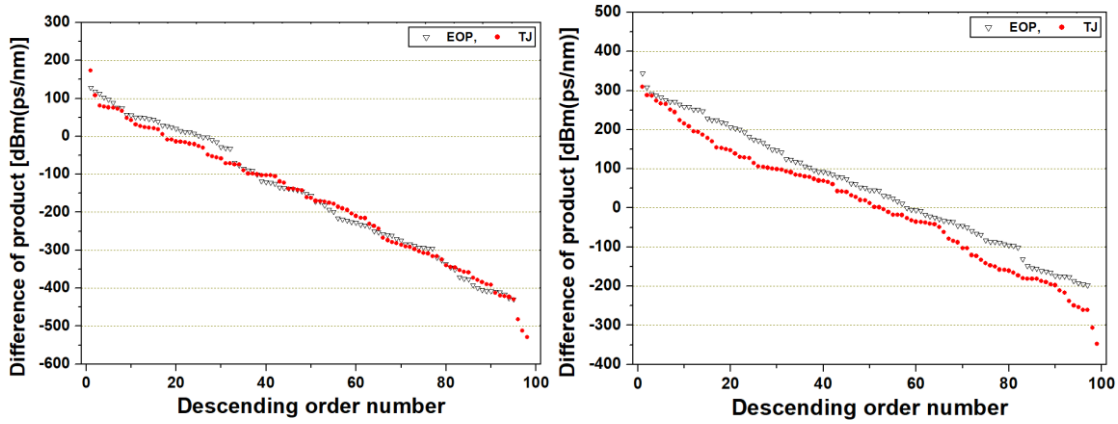

Figure 4. The difference in product based on EOP and TJ. (a) 23-27 configuration, and (b) 27-23 configuration.

Similar to the power margin analysis in Figure 3, the performance evaluation using the 'product' was conducted by calculating the difference relative to the product obtained from a uniform distribution link. Consistent with the observations in Figure 3, both assessments reveal that the 27-23 configuration yields superior compensation performance compared to the 23-27 configuration.

 doi:10.20944/preprints202603.2159.v1

However, in contrast to the results shown in Figure 2, the deviations in amplitude and phase compensation for distorted signals are found to be more significantly reduced in the 23-27 configuration than in the 27-23 configuration.

Since the evaluations of both the power margin and the product are presented relative to the performance of the uniform distribution link, the random RDPS patterns that yield positive values on the y-axis in Figures 3 and 4 can be considered effective for practical link applications. A visual inspection of Figures 3 and 4 confirms that the 27-23 configuration possesses a larger number of random distribution patterns that achieve effective compensation compared to the 23-27 configuration. However, a more rigorous analysis reveals that the specific random patterns yielding superior compensation vary depending on the OPC location, the evaluation metrics (i.e., EOP and TJ), and the performance factors (i.e., power margin and product). This variability suggests that the identification of a universally optimal dispersion map may present significant challenges for practical implementation.

The findings of this study confirm that while the randomization of RDPS distribution across all fiber spans generally falls short of the compensation performance achieved by uniform or deterministic (artificial) methods, it does provide significant compensation effects for specific random patterns. We anticipate that identifying the common characteristics of these specific patterns and applying them to link design would be a worthwhile endeavor, particularly for ensuring design flexibility in the dispersion-managed links. Establishing these underlying principles could provide a more robust and adaptable framework for future optical transmission systems.

The identification of the specific characteristics of random RDPS distributions that offer enhanced compensation compared to uniform distribution links can be initiated by building on our previous research findings. Leveraging these prior results will serve as a foundational starting point for identifying the underlying patterns that consistently outperform conventional configurations. A key finding from our previous research is that when employing a dispersion map to compensate for WDM signal distortion in an OPC-aided transmission link, the specific shape of the dispersion profile significantly influences the compensation quality.

Through numerical investigations of various dispersion maps, it was identified that the compensation efficacy improves as the dispersion profile becomes more symmetrical with respect to the OPC. In particular, we confirmed that distortion compensation is notably superior in links where an antipodal-symmetric profile, as opposed to simple bilateral symmetry, is applied.

Figure 5 illustrates four types of dispersion maps with antipodal-symmetric distributions that can be applied to the 23-27 configuration links using the aforementioned RDPS. While it is certainly possible to design more than four types of antipodal-symmetric dispersion maps, we have focused on the four shown in Figure 5 to derive the common characteristics of random patterns that optimize compensation, specifically considering the number of fiber spans and the types of RDPS employed in this study.

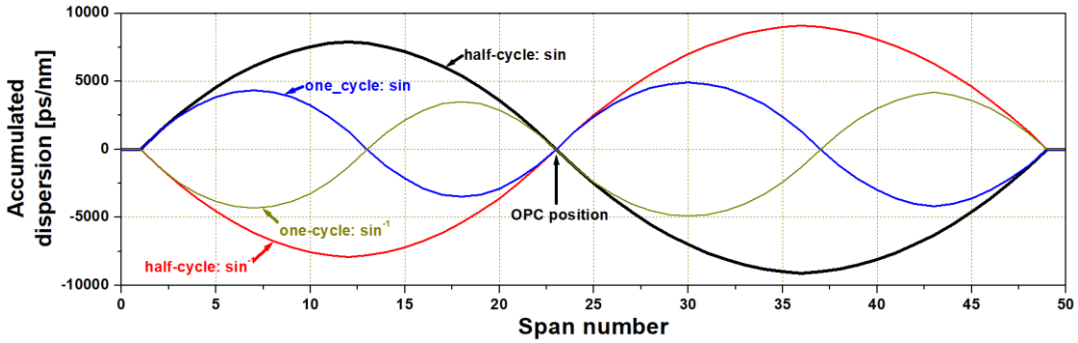

Figure 5. Four dispersion maps can create the antipodal symmetry with respect to OPC.

 doi:10.20944/preprints202603.2159.v1

Although all four dispersion maps follow a sinusoidal profile, they are distinguished by how the former and latter sections are symmetrically opposed relative to the position of the OPC. Due to the nature of antipodal symmetry, the cumulative dispersion profiles before and after the OPC are inverted versions of each other; thus, each map's characteristics can be uniquely identified by the shape of the former section profile alone. The maps are categorized based on two primary criteria: 1) whether the cumulative profile in the former section follows a standard sine wave or an inverted sine wave, and 2) whether the repetition period consists of a full cycle or a half cycle. Accordingly, these configurations are labeled as 'one-cycle:sine', 'half-cycle:sine', 'one-cycle:sine^{-1}', and 'half-cycle:sine^{-1}'.

The reason we considered the four dispersion maps in Figure 5 stems from the hypothesis that, although the dispersion profiles derived from the 100 random distributions are inherently irregular, each may closely resemble one of the four reference profiles. Based on this premise, the process for identifying common characteristics within the RDPS was conducted as follows. First, the similarity between each of the 100 random-based dispersion maps and the four reference maps was quantified. The Pearson correlation coefficient was employed for this comparison. Weights were then assigned in descending order—with a decrement of '1' between consecutive ranks—from the most highly correlated random pattern to the least.

The next step involved identifying and ranking the random patterns that demonstrated superior performance across all four examined metrics: the power margin and product based on EOP, and the power margin and product based on TJ. Finally, the similarity weights of the top 10 performing random patterns were mapped to the four symmetric dispersion maps shown in Figure 5. By summing these weights for each symmetric structure, we identified which of the four maps the top-performing random patterns most closely resembled.

Figures 6(a,b) show the eye diagrams resulting from uniform distribution structures for the 23-27 and 27-23 configurations. In contrast, Figures 6(c–f) depict the eye diagrams obtained under random pattern conditions that yielded the best and poorest compensation performance for these links. For the 23-27 configuration, the Pearson correlation coefficients between Random Pattern #99, which yielded the optimal compensation, and the four symmetric distributions—one-cycle: sine, half-cycle: sine, one-cycle: sine^{-1}, and half-cycle: sine^{-1}—were 0.078, 0.035, -0.078, and -0.035, respectively. The corresponding weights for these values were 75, 44, 26, and 57. Contrary to our initial expectations, these results indicate a low degree of similarity with the four aforementioned antipodal-symmetric distributions.

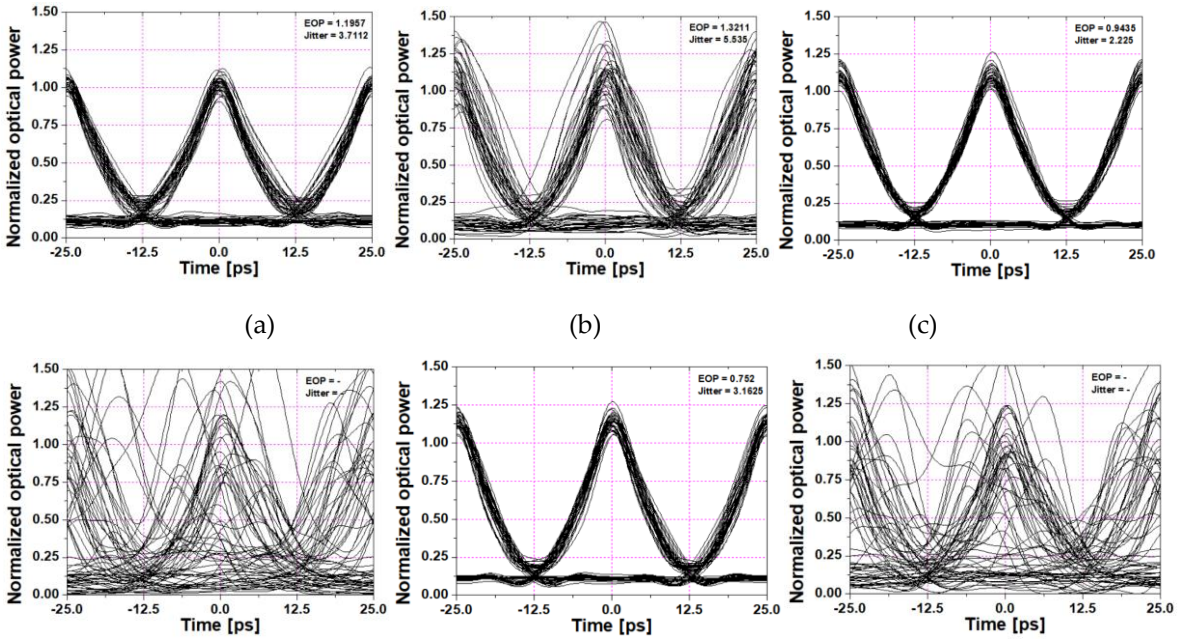

 doi:10.20944/preprints202603.2159.v1

(d) (e) (f)

Figure 6. The eye diagrams. (a) uniform distribution in 23-27 configuration and (b) 27-23 configuration, (c) best compensation by random number 99 and (d) worst compensation by random number 66 in 23-27 configuration, (e) best compensation by random number 51 and (f) worst compensation by random number 66 in 27-23 configuration.

Through iterative trials utilizing this methodology, it became evident that the current analytical framework exhibited inherent limitations that might compromise the validity of the results. Specifically, while the identification of best and worst compensation patterns was intended to integrate EOP- and TJ-based power margins and products, the compensation efficacy within a given distribution showed significant inconsistency across the metrics. Consequently, establishing a consistent weighting system was hindered by the non-uniform performance of the patterns relative to each indicator. To minimize these potential errors, we deliberately expanded our scope by considering ten different random patterns capable of achieving optimal compensation, rather than relying on a single representative pattern.

Table 1 summarizes the weights and the resulting sums of the Pearson correlation coefficients between the dispersion maps generated by the top ten random patterns—which achieved superior compensation in each system—and each of the four antipodal- symmetric dispersion maps. Here, the 'sum' represents the total of the ten weights calculated for each specific antipodal symmetric distribution. In both systems, the highest 'sum' was observed for the 'half-cycle: sine' configuration.

Table 1. The weights and their respective sums of the Pearson correlation coefficient.

Random No.	weighting in 27-23 link				Random No.	weighting in 27-23 link			
	half-cycle		one-cycle			half-cycle		one-cycle	
	sin	$\sin^{-1}$	sin	$\sin^{-1}$		sin	$\sin^{-1}$	sin	$\sin^{-1}$
99	58	43	72	29	51	80	21	89	12
25	88	13	24	77	90	67	34	18	83
32	74	27	66	36	55	35	66	66	35
20	35	66	35	66	18	65	36	64	37
40	99	2	85	16	10	84	17	53	48
5	15	86	61	40	99	44	57	75	26
34	63	38	1	100	2	42	59	71	30
77	70	31	80	21	14	31	70	13	88
51	49	52	67	34	1	46	55	63	38
4	20	81	21	80	34	39	62	3	98
Sum	571	439	512	499	Sum	533	477	515	495

These results indicate that for both the 23-27 and 27-23 configurations, achieving a superior compensation effect requires the overall shape of the dispersion map—generated by the random RDPS distribution—to more closely resemble the 'half-cycle: sine' profile compared to the other three antipodal symmetric distributions. This confirms that even in dispersion links where RDPS is randomly assigned to each fiber span, intentional intervention in the allocation process is essential. Specifically, distributing the RDPS such that the dispersion map approximates 1-cycle sine wave—characterized by a positive half-cycle in the former section and a negative half-cycle in the latter

 doi:10.20944/preprints202603.2159.v1

section relative to the OPC—is pivotal for achieving optimal compensation of distorted WDM channels.

The dispersion maps associated with the three best-performing random distributions for the 23-27 and 27-23 configurations are illustrated in Figures 7(a-b). In these figures, the patterns exhibiting the highest similarity to the 'half-cycle: sine' structure (Pattern No. 70 for the 23-27 configuration and No. 23 for the 27-23 configuration) are also plotted for comparison. Unlike the patterns that strictly follow the 'half-cycle: sine' shape, the maps yielding the most effective compensation exhibit subtle variations in their accumulated dispersion across individual fiber spans. Despite these minor fluctuations, a consistent feature across both links is the distinct demarcation of accumulated dispersion—maintaining a positive trend pre-OPC and a negative trend post-OPC.

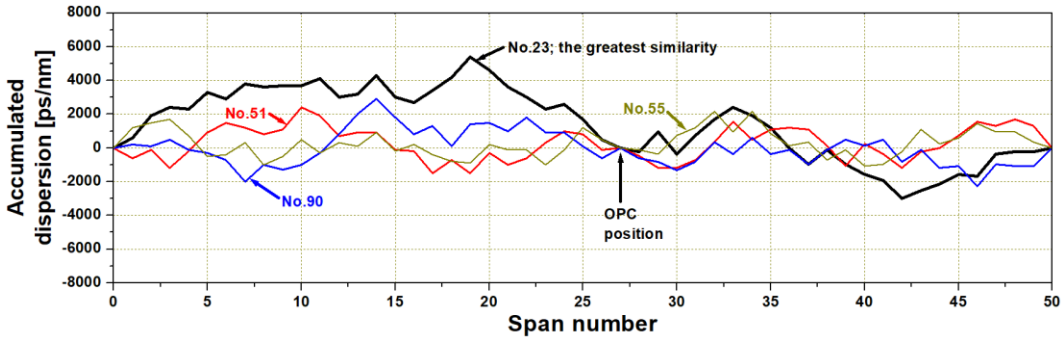

(a)

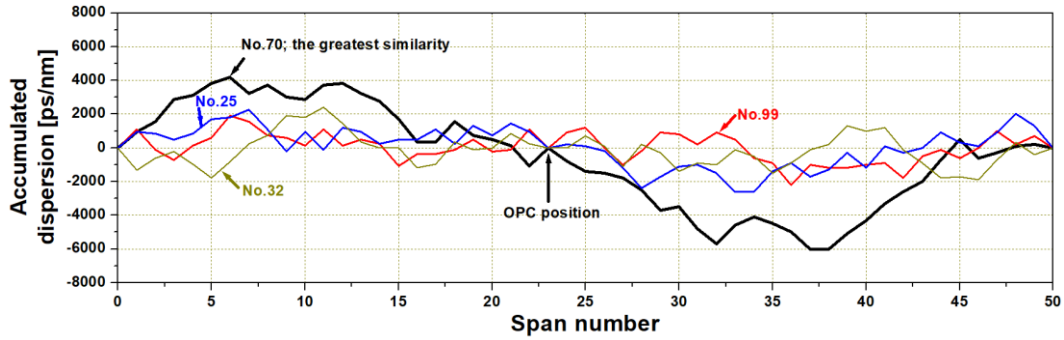

(b)

Figure 7. The dispersion maps for analysis.

5. Conclusions

In this study, we performed a comprehensive numerical investigation of dispersion-managed DWDM transmission systems incorporating a non-midway OPC with randomly distributed RDPS. Unlike conventional studies assuming idealized, symmetric configurations, this work focused on realistic transmission environments where OPC placement is asymmetric and dispersion distribution is inherently random.

The simulation results revealed that OPC positioning exerts a significant influence on compensation performance. In particular, the 27–23 configuration—where the OPC is located closer to the receiver—generally provided superior compensation in terms of both power margin and system-wide tolerance compared to the 23–27 configuration. This indicates that the asymmetric placement of OPC can be strategically utilized to enhance system performance, even in non-ideal conditions.

Furthermore, although randomly distributed RDPS does not consistently outperform uniform or artificially designed dispersion maps, certain random patterns were found to achieve comparable or even improved compensation performance. These findings suggest that randomness itself is not

 doi:10.20944/preprints202603.2159.v1

inherently detrimental; rather, specific structural characteristics within the random dispersion maps play a critical role in determining system efficacy.

Correlation analysis with representative antipodal-symmetric dispersion profiles revealed that high-performing random patterns tend to resemble half-cycle sinusoidal dispersion maps. Specifically, we identified that keeping the accumulated dispersion positive pre-OPC and negative post-OPC serves as a pivotal factor in achieving optimal compensation. These findings underscore that even in random RDPS environments, incorporating intentional structural guidance can significantly improve system performance.

Overall, this work provides practical design insights for dispersion-managed optical transmission systems under realistic constraints. The results suggest that while achieving optimal performance through rigid deterministic design is significant, it can also be attained by guiding random dispersion distributions toward favorable structural patterns, thereby enhancing design flexibility. These findings contribute to the development of more flexible and robust design strategies for future high-capacity optical communication systems incorporating non-midway OPC.

Author Contributions: Conceptualization, J-P.C. and S-R.L.; methodology, S-R.L.; software, S-R.L.; analysis, J-P.C. and S-R.L.; resources, S-R.L.; data curation, S-R.L.; writing—original draft preparation, J-P.C. and S-R.L.; writing—review and editing, J-P.C. and S-R.L.; visualization, S-R.L.; super-vision, J-P.C. and S-R.L.; project administration, S-R.L. All authors have read and agreed to the published version of the manuscript.

Funding: Please add: This research received no external funding.

Institutional Review Board Statement: Not applicable.

Informed Consent Statement: Informed consent was obtained from all subjects involved in the study.

Data Availability Statement: The data presented in this study are available on request from the corresponding author. The data are not publicly available due to Institutional regulations.

Conflicts of Interest: The authors declare no conflict of interest regarding the publication of this paper.

References

1. Secondini, M.; Forestieri, E., Scope and limitations of the nonlinear Shannon limit, *J. Lightwave Technol.* 2016, *35*, 893–902. **DOI:** 10.1109/JLT.2016.2620721.
2. Kareem, A.H.A.; Murdas, I.A., **Performance evaluation of fiber impairment mitigation for high capacity communication systems using optical compensation method,** *Results in Opt. 2023, 11,* 100399, DOI: https://doi.org/10.1016/j.rio.2023.100399
3. Sabapathi, T.; Poovitha, R., **Mitigation of nonlinearities in fiber optic DWDM system,** *Optik.* 2019, 657-664, DOI: https://doi.org/10.1016/j.ijleo.2019.02.073
4. Abu-Romoh, M.; Costa, N.; Jaouën, Y.; Napoli, A.; Pedro, J.; Spinnler, B.; Yousefi, M., Equalization in dispersion-managed systems using learned digital back-propagation, arXiv:2307.06821. DOI: https://doi.org/10.48550/arXiv.2307.06821
5. Dany, B.; Leclerc, O.; Neddam, F.; Le Lourec, P., Optimization of 40 Gbit/s dispersion maps for long-haul WDM transmissions with up to 0.4 bit/s/Hz spectral efficiency, I**n** 2001 Optical Fiber Communication Conference and Exhibit, Technical Digest Postconference Edition (IEEE Cat. 01CH37171), Anaheim, CA, USA, **DOI:** 10.1109/OFC.2001.927353
6. Keykhosravi, K.; Secondini, M.; Durisi, G.; Agrell, E., How to increase the achievable information rate by per-channel dispersion compensation. *J. Lightwave Technol.* 2019, *37*, 2443–2451. DOI: https://opg.optica.org/jlt/abstract.cfm?URI=jlt-37-10-2443.
7. Yao-Jun, Q.; Xue-Jun, L.; Yue-Feng, J., Fiber nonlinearity post-compensation by optical phase conjugation for 40Gb/s CO-OFDM systems, *Chinese Phys. Lett.* 2011, *28*, 064214. DOI: 10.1088/0256-307X/28/6/064214.

 doi:10.20944/preprints202603.2159.v1

8. Liu, X.; Qiao, Y.; Ji, Y., Reduction of the fiber nonlinearity impairment using optical phase conjugation in 40 Gb/s CO-OFDM systems, *Opt. Commun.* 2010, *283*, 2749-2753, DOI: https://doi.org/10.1016/j.optcom.2010.03.015
9. Ali, A. A. I.; Costa, C. S.; Al-Khateeb, M. A. Z.; Ferreira, F. M.; Ellis, A. D. An expression for nonlinear noise in optical phase conjugation systems with lumped amplifiers. *IEEE Photonics Technol. Lett*. 2018, *30*, 2056–2059. **DOI:** 10.1109/LPT.2018. 2876376.
10. Kaminski, P.M. ; Da Ros, F.; Yankov, M.P.; Clausen, A.T.; Forchhammer, S.; Oxenløwe, L.K.; Galili, M., Symmetry enhancement through advanced dispersion mapping in OPC-aided transmission *J. Lightwave Technol*. **2021,** *39*, 2820-2829, DOI: https://opg.optica.org/jlt/abstract.cfm?URI=jlt-39-9-2820
11. Mohs, G.; Anderson, W. T.; Pilipetskii, A.; Golovchenko, E. A., Enhanced submarine transmission fiber enabling novel dispersion maps and improved system performance. *IEEE Photonics Technol. Lett*. 2011, 23, 636 –638. **DOI:** 10.1109/LPT.2011.2120604
12. Chung, J-P.; Lee, S-R. Dispersion-managed link configured with repetitively shaped dispersion maps and embedded with mid-span spectral inversion, *J. Inf. Commun. Converg. Eng*. 2022. *20*, 235–241, DOI: https://doi.org/10.56977/jicce.2022.20.4.235.
13. Chung, J.-P.; Lee, S.-R., MSSI-based dispersion-managed link configured by randomly-distributed RDPS only in former half section. *Appl. Sci*. 2022, 12, 8970. DOI: https://doi.org/10.3390/app12188970.
14. Chung, J.-P.; Lee, S.-R., MSSI system combined with dispersion-managed link configured with random-based RDPS differently controlled by fiber length, *Appl. Sci*. 2024, 14, 9722. DOI: https://doi.org/10.3390/app14219722
15. Chung, J.-P.; Lee, S.-R., Dispersion-managed optical link configured antipodal symmetric dispersion maps with respect to midway optical phase conjugator, *J. lnf. Commun. Converg. Eng*. 2023, 21, 103-109, DOI: https://doi.org/10.56977 /jicce.2023.21.2.103
16. Minzioni, P.; Schiffini, A., Unifying theory of compensation techniques for intrachannel nonlinear effects. *Opt. Express* 2005, *13*, 8460–8468, 2005. DOI: https://doi.org/10.1364/OPEX.13.008460.
17. Tang, X; Wu, Z., Suppressing modulation instability in midway optical phase conjugation systems by using dispersion compensation. *IEEE Photonics Technol. Lett*. 2005, *17*, 926 – 928. **DOI:** 10.1109/LPT.2004.843275